RESEARCH ARTICLE SUMMARY

SIGNAL TRANSDUCTION

In vivo brain GPCR signaling elucidated by phosphoproteomics

Jeffrey J. Liu, Kirti Sharma, Luca Zangrandi, Chongguang Chen, Sean J. Humphrey, Yi-Ting Chiu, Mariana Spetea, Lee-Yuan Liu-Chen, Christoph Schwarzer*, Matthias Mann*

INTRODUCTION: The G protein–coupled receptor (GPCR) superfamily is a major drug target for neurological diseases. Functionally selective agonists activate GPCRs, such as the kappa opioid receptor (KOR), in a pathway-specific manner that may lead to drugs with fewer side effects. For example, KOR agonists that trigger beneficial antinociceptive, antipruritic, and anticonvulsant effects while causing minimal or no undesirable dysphoric, aversive, or psychotomimetic effects would be invaluable in light of the current opioid epidemic. However, functional selectivity observed in vitro frequently has little predictive value for behavioral outcomes.

RATIONALE: Obtaining a systems view of GPCR signaling in the brain may overcome the gap between in vitro pharmacology and in vivo testing. Recent breakthroughs in mass spectrometry–based proteomics have enabled us to quantify tens of thousands of phosphorylation events simultaneously in a high-throughput fashion. Using the KOR as a GPCR model, we applied this technology to achieve a global overview of the architecture of brain phosphoproteome in five mouse brain regions, in which we examined signaling induced by structurally and behaviorally diverse agonists.

RESULTS: Through the quantification of 50,000 different phosphosites, this approach yielded a brain region–specific systems view of the phosphoproteome, providing a context to understand KOR signaling in vivo. We observed strong regional specificity of KOR signaling attributable to differences in protein-protein interaction networks, neuronal contacts, and the different tissues in neuronal circuitries. Agonists with distinct signaling profiles elicited differential dynamic phosphorylation of synaptic proteins, thereby linking GPCR signaling to the modulation of brain functions. The most prominent changes occurred on synaptic proteins associated with dopaminergic, glutamatergic, and γ-aminobutyric acid–mediated (GABAergic) signaling and synaptic vesicle release. The large-scale dephosphorylation of synaptic proteins in the striatum after 5 min of agonist stimulation was partially blocked by protein phosphatase 2A (PP2A) inhibitors, underscoring the involvement of PP2A in KOR-mediated synaptic functions. Pathway analysis revealed enrichment of mTOR (mechanistic target of rapamycin) signaling by agonists associated with aversion. Strikingly, mTOR inhibition during KOR activation abolished aversion while preserving therapeutic antinociceptive and anticonvulsant effects. Parallel characterization of phosphoproteomic changes related to KOR-mediated mTOR activation in a cell line model provided additional mechanistic insights at the level of the signaling cascade.

ON OUR WEBSITE

Read the full article at http://dx.doi.org/10.1126/science.aao4927

CONCLUSION: We dissected the signaling pathways associated with desired and undesired outcomes of KOR activation in vivo and applied this knowledge to suppress the latter. Our work demonstrates the utility of combining phosphoproteomics with pharmacological tools and behavioral assessments as a general approach for studying GPCR signaling in vivo. Together with appropriate in vitro cellular systems, individual pathways can be characterized in depth, providing a rational basis for GPCR drug discovery. ■

The list of author affiliations is available in the full article online.
*Corresponding author. Email: mmann@biochem.mpg.de (M.M.); schwarzer.christoph@i-med.ac.at (C.S.)
Cite this article as J. J. Liu *et al.*, *Science* **360**, eaao4927 (2018). DOI: 10.1126/science.aao4927

High-throughput phosphoproteomics to characterize in vivo brain GPCR signaling. Subsequent bioinformatic analysis enables prediction and modulation of downstream signaling pathways, which are correlated with unwanted effects but not the therapeutic outcome.

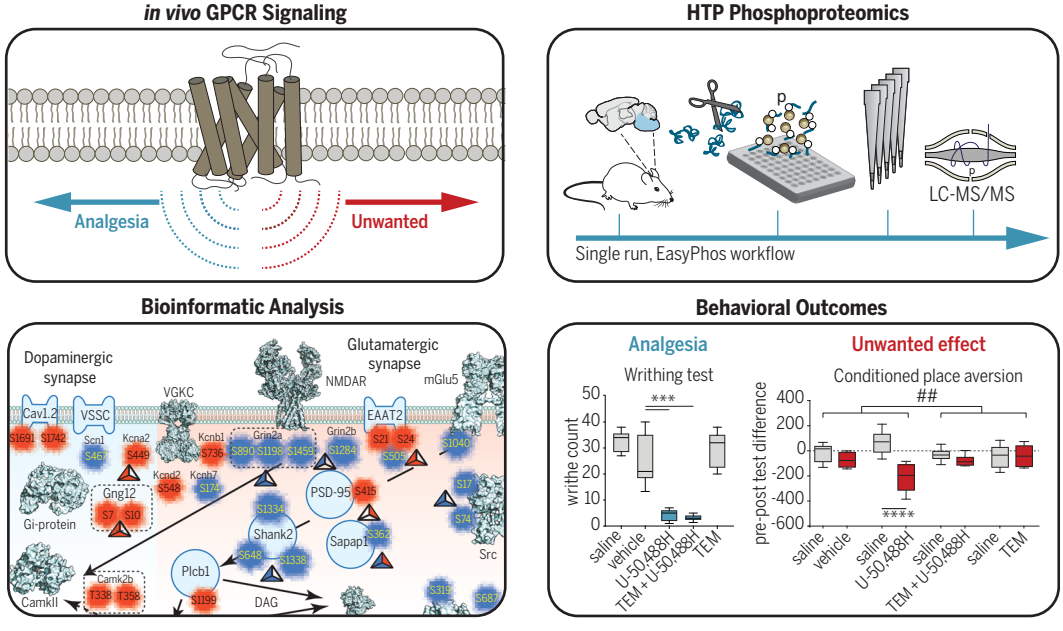

RESEARCH ARTICLE

SIGNAL TRANSDUCTION

In vivo brain GPCR signaling elucidated by phosphoproteomics

Jeffrey J. Liu[1], Kirti Sharma[1], Luca Zangrandi[2], Chongguang Chen[3], Sean J. Humphrey[1], Yi-Ting Chiu[3], Mariana Spetea[4], Lee-Yuan Liu-Chen[3], Christoph Schwarzer[2]*, Matthias Mann[1,5]*

A systems view of G protein–coupled receptor (GPCR) signaling in its native environment is central to the development of GPCR therapeutics with fewer side effects. Using the kappa opioid receptor (KOR) as a model, we employed high-throughput phosphoproteomics to investigate signaling induced by structurally diverse agonists in five mouse brain regions. Quantification of 50,000 different phosphosites provided a systems view of KOR in vivo signaling, revealing novel mechanisms of drug action. Thus, we discovered enrichment of the mechanistic target of rapamycin (mTOR) pathway by U-50,488H, an agonist causing aversion, which is a typical KOR-mediated side effect. Consequently, mTOR inhibition during KOR activation abolished aversion while preserving beneficial antinociceptive and anticonvulsant effects. Our results establish high-throughput phosphoproteomics as a general strategy to investigate GPCR in vivo signaling, enabling prediction and modulation of behavioral outcomes.

The G protein–coupled receptor (GPCR) superfamily encompasses drug targets in numerous therapeutic areas, including cancer (*1*) and cardiac (*2*) and neurological (*3*) diseases. Stimulation of a single GPCR, such as the kappa opioid receptor (KOR), often activates parallel pathways, each leading to distinctive pharmacological outcomes. For example, KOR activation triggers beneficial analgesic (*4*), antipruritic (*5*, *6*), and anticonvulsant/antiepileptic (*7*) signaling (*8*) as well as undesirable dysphoria or aversion and psychotomimetic effects (*8*, *9*) (Fig. 1A). Recently, some KOR agonists were described that do not induce conditioned place aversion (CPA) in mice (*10*, *11*), in contrast to endogenous and classical agonists. Functional selectivity, a GPCR signaling paradigm derived from in vitro (*12*, *13*) and structural (*14*, *15*) experiments, was used to explain this phenomenon (*16*, *17*). However, functional selectivity in cells transfected with KOR is not directly translatable to cells naturally expressing KOR (*18*) or to behavioral effects in vivo (*19*). The complexity of brain circuitry hinders the in vitro–in vivo correlation through heterogeneity at protein, cellular, and neural pathway levels (*20*). Thus, it is imperative to develop an unbiased approach that directly investigates GPCR (and specifically KOR) signaling in vivo, thereby elucidating the largely elusive downstream signaling consequences of GPCR activation in the brain.

Developments in mass spectrometry (MS)–based proteomics in general, and phosphoproteomics in particular, now enable the near-comprehensive characterization of proteomes and tens of thousands of phosphorylation events (*21*–*24*). Application of MS to study GPCR signaling has been limited to assaying the phosphorylation state of a single receptor (*25*) or small-scale phosphoproteomics on in vitro cell lines (*26*–*28*) or ex vivo cells (*29*). We recently described the EasyPhos technology, which streamlines phosphoproteomics to such an extent that hundreds of phosphoproteomes can be measured in a short time and at uncompromised depth of coverage, enabling time-course studies of dynamic and signaling events in vivo (*30*, *31*). Here, we applied this technology along with behavioral and pharmacological investigations to attain a systems view of KOR signaling induced by diverse agonists in temporally and spatially resolved areas of the mouse brain.

Brain phosphoproteomic architecture

We administered five KOR agonists intracisternally (i.c.) in dosages established to be effective in pharmacological and behavioral experiments (Fig. 1B and Table 1). After short (5 min) and long (30 min) intervals after injection, we dissected four brain regions that express KOR at different levels (striatum, hippocampus, cortex, and medulla oblongata) and one without detectable KOR expression (cerebellum) (Fig. 1C). In total, including biological replicates (three per experimental condition) and follow-up experiments, we measured more than 300 single-shot label-free phosphoproteomic samples using the high-throughput EasyPhos platform (*30*) (Fig. 1D). Together, this yielded more than 60,000 different identified phosphosites mapping to ~6700 brain proteins. This is the most comprehensive coverage of any organ phosphoproteome reported to date, underscoring the diversity and importance of phosphorylation-based regulation in the brain (Fig. 1E).

To obtain a general overview of the architecture of the brain phosphoproteome, we performed principal components analysis (PCA), which revealed that the phosphoproteomes of each brain region cluster tightly and are distinct from other regions. This indicates that each region possesses a unique phosphoproteome signature. Furthermore, brain regions that share a similar developmental origin exhibit similarities in their phosphoproteome (Fig. 2A, component 2). The region-specific nature of the phosphoproteome is partly driven by the underlying differences in the proteomes, because proteins highly expressed in one brain region (e.g., striatum) often also yield prominent phosphopeptides in the same region (Fig. 2, B and C). In particular, expression levels of kinases (*32*) (the "kinome") correlated significantly with the abundance of phosphopeptides containing the corresponding linear motifs (Fig. 2D). Thus, proteome and kinase expression in different regions partially shapes the brain phosphoproteome. The complexity within the brain phosphoproteome is in contrast to the homogeneity of in vitro cell lines. We observed that 85% of synaptic proteins were phosphorylated, which is of particular interest given previous reports of the importance of phosphorylation in the regulation of synaptic plasticity (*33*).

Approximately 50,000 of the identified phosphorylation sites were quantifiable (Fig. 1F). As established in our recent studies using EasyPhos technology, reproducibility between biological replicates was robust, with an average Pearson correlation of ~0.85 (fig. S1). Injection of the reference KOR agonist U-50,488H significantly perturbed ~5% of these sites, with different ligand perturbation patterns in distinct brain regions (Fig. 1G). After 5 min of U-50,488H stimulation, we observed maximum perturbation in the striatum (1000 sites), and progressively less in the order of hippocampus > cortex > medulla oblongata, in line with the expression level of KOR in the respective brain regions (*34*). In the cerebellum, where KOR is not detectable, there were hardly any regulated sites, providing a strong validation of our technology (Fig. 1G). Furthermore, we found that in the four KOR-expressing brain regions (striatum, hippocampus, cortex, and medulla oblongata), the regulated sites were not detected in the brains of KOR knockout mice (KOR-KO), which demonstrates the specificity of ligand effects in the brain (fig. S2). Overall, these results show that phosphoproteomics

[1]Department of Proteomics and Signal Transduction, Max Planck Institute of Biochemistry, 82152 Martinsried, Germany. [2]Department of Pharmacology, Medical University of Innsbruck, 6020 Innsbruck, Austria. [3]Center for Substance Abuse Research and Department of Pharmacology, Temple University Lewis Katz School of Medicine, Philadelphia, PA 19140, USA. [4]Department of Pharmaceutical Chemistry, Institute of Pharmacy and Center for Molecular Biosciences Innsbruck (CMBI), University of Innsbruck, 6020 Innsbruck, Austria. [5]Novo Nordisk Foundation Center for Protein Research, Faculty of Health Sciences, University of Copenhagen, 2200 Copenhagen, Denmark.
***Corresponding author. Email: mmann@biochem.mpg.de (M.M.); schwarzer.christoph@i-med.ac.at (C.S.)**

enables observation of KOR-modulated signaling in a brain region–specific fashion.

KOR signaling is brain region–specific

Next, we spatially and temporally analyzed U-50,488H–regulated sites determined to be significant by analysis of variance (ANOVA). U-50,488H activates inhibitory G proteins ($G_{i/o}$) and induces internalization of KOR through β-arrestin2 recruitment (*35*). Inhibition of Ca^{2+} channels modulates release of neurotransmitters such as γ-aminobutyric acid (GABA), dopamine, and glutamate, and negatively regulates signaling mediated by all three neurotransmitters. Accordingly, our bioinformatics analysis of regulated phosphosites (*36*) revealed significant enrichment of Gene Ontology (GO) terms such as "inhibition of adenylate cyclase activity by G protein signaling pathway," "positive regulation of receptor internalization," and "regulation of neurotransmitter secretion." This unbiased approach also highlighted mechanisms not yet linked to KOR activation, such as "RNA splicing" (fig. S3A). In line with this, the phosphorylation states of numerous membrane proteins, such as voltage-gated sodium channels and neurotransmitter transporters, are altered by KOR activation (fig. S3B).

Like the basal brain phosphoproteome, phosphosites clustered tightly by replicates. Interestingly, the PCA map was dynamic in time, with the relative positions of the cortex, medulla, hippocampus, and striatum changing drastically between the time points (Fig. 3, A and B). In the first component, the striatum deviated most from the other regions at the 5-min interval, whereas the cortex diverged mostly at 30 min, which suggests that U-50,488H perturbation is most profound in the striatum at early time points and in the cortex at later time points. The striatum is part of the mesolimbic pathway and the cortex is part of the mesocortical pathway; these are the two most prominent pathways in KOR signaling (also reflected in the relatively high KOR expression in both regions). Unlike in vitro cell model systems, each brain region comprises elaborated connections of heterogeneous neurons. In this complex background, we also discovered U-50,488H–mediated KOR signaling to be highly region-specific. For example, we found that U-50,488H–regulated sites in the striatum were specific to this region—a result that also held for the other brain regions (Fig. 3C and fig. S4).

At the level of known functional sites, we observed dephosphorylation of the dopamine- and cyclic adenosine monophosphate (cAMP)–regulated neuronal phosphoprotein (DARPP-32) on phosphorylated Ser^{97} (pS97) and of the tyrosine kinase Src on pS17 exclusively in the striatum. The *raf* proto-oncogene serine/threonine protein kinase Raf1 was dephosphorylated at pS259 only in the cortex, and the extracellular signal–regulated kinase ERK1 was phosphorylated at Thr^{203} and Tyr^{205} (pT203/pY205) only in the hippocampus (Fig. 3D). We further investigated the regional specificity of ERK1 phosphorylation using immunohistochemistry. This latter observation validates the phosphoproteomics findings and reveals that elevated ERK1 phosphorylation is specifically located on hippocampal mossy fibers (Fig. 3E).

In contrast to the basal phosphoproteome, which was partly shaped by the proteome and particularly by the kinome (Fig. 2), no correlation between U-50,488H–regulated phosphorylation events and the region-specific proteome or basal phosphoproteome was observed (fig. S5). This implies that region-specific regulation is not just a function of expression levels of kinases and substrates, but results from more complex factors such as different protein-protein interaction networks, neuronal contacts, or the position of the tissue in neuronal circuitries. Indeed, mapping the U-50,488H–regulated phosphorylation events onto known interaction networks (*37*) highlighted the signaling pathways relevant to the specific physiological functions of each brain region, including the GO terms "neurotransmitter secretion" and "dopaminergic synapses" (enriched in striatum) and "axon guidance," "long-term potentiation," and "calcium signaling" (enriched in hippocampus), which was not the case for the basal phosphoproteome (fig. S6).

Next, we contrasted signaling of the initially investigated agonist U-50,488H with that of 6′GNTI (*38*), which possesses a different signaling profile (Table 1). Depending on the brain region and time point, U-50,488H and 6′GNTI shared 30 to 50% of regulated sites. Substantial differences were apparent in the first component of a PCA between U-50,488H and 6′GNTI after 5 min of stimulation in the striatum and hippocampus, but not in the medulla oblongata and cortex. After 30 min of stimulation, the ligand differences were greatly reduced in the striatum but were more pronounced in other regions, especially the cortex (fig. S7). Because the i.c. injected doses of each ligand were similar across brain regions and time points, these region- and time-dependent changes between ligands may reflect the position of the regions in distinct brain circuitry, but also may reflect differences in pharmacokinetic effects and biodistribution of these two agonists.

KOR signaling in the striatal synaptic phosphoproteome

Some KOR agonists induce aversive states, primarily through activation of medium spiny neurons in the nucleus accumbens (NAc) of the

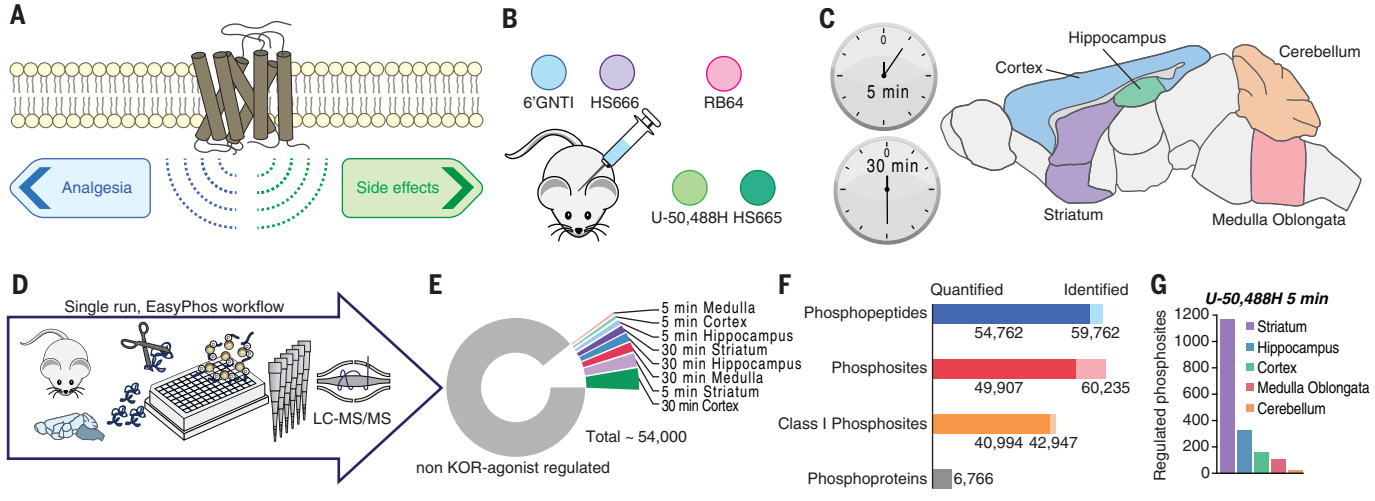

Fig. 1. High-throughput phosphoproteomics of in vivo KOR-mediated GPCR signaling. (**A**) KOR signaling activates antinociception while inducing unwanted side effects. (**B**) Five KOR agonists were administrated i.c. to mice with U-50,488H as the reference KOR agonist. (**C**) Drug-treated groups of mice were killed 5 or 30 min after injection in each experimental group (n = 3 per group). Five brain regions were dissected and processed for phosphoproteomic studies. (**D**) The single-run EasyPhos workflow. (**E**) Of ~50,000 quantifiable phosphosites, fewer than 5% were perturbed by the U-50,488H treatment. (**F**) Overall statistics of the brain phosphoproteome. (**G**) The magnitude of U-50,488H–induced perturbation differs among brain regions. The striatum has the most detectable perturbation with more than 1000 sites, whereas the cerebellum has fewer observable U-50,488H–induced perturbation.

Table 1. KOR ligands: In vitro pharmacological profiles and behavioral responses. Conditioned place aversion is designated "yes" or "no" depending on whether it was observed at the dosage applied in the present phosphoproteomic experiments. The applied dose is that used in the present study. EC_{50}, concentration of the ligand at half of the maximal response; E_{max}, maximal response elicited from a given ligand; n.a., not available.

Ligands	Binding affinity, human KOR	G protein activation, human KOR		β-arrestin2 recruitment, human KOR		Conditioned place aversion	Anticonvulsant effect (range)	Antinociceptive effect (range)	Applied dose (nmol)
	K_i (nM)	EC_{50} (nM)	E_{max} (%)	EC_{50} (nM)	E_{max} (%)				
U-50,488H	0.68 (*71*)	43 (*38*)	100 (*38*)	2 (*38*)	100 (*38*)	Yes (100 nmol) (*11*) Yes (2.5 mg/kg) (*7*)	6 to 20 mg/kg (*7*)	3 to 10 nmol (*11*) 1 to 5 mg/kg (*44*)	20
6′GNTI	1.15 (*72*)	1.6 (*38*)	64 (*38*)	n.a. (*38*)*	n.a. (*38*)*	No (1 to 30 nmol) (*7*)	3 to 30 nmol (*7*)	10 nmol (*73*)	30
RB64	0.59 (*74*)	5.29 (*60*)	101 (*60*)	391 (*60*)	104 (*60*)	Yes (3 mg/kg) (*9*)	n.a.	3 mg/kg (*9*)	3†
HS665	0.49 (*55*)	3.62 (*55*)	90.0 (*55*)	463 (*11*)	55 (*11*)	Yes (30 nmol) (*11*)	n.a.	3 to 10 nmol (*11*) 1.25 to 5 mg/kg (*44*)	10
HS666	5.90 (*55*)	35.0 (*55*)	53.4 (*55*)	449 (*11*)	24 (*11*)	No (150 nmol) (*11*)	n.a.	3 to 30 nmol (*11*) 2 to 10 mg/kg (*75*)	30

*EC_{50} and E_{max} for β-arrestin2 recruitment of 6′GNTI are controversial and reported with different values in the literature. EC_{50} = 5.9 nM and E_{max} = 12% (*18*), and EC_{50} = 7.38 nM and E_{max} = 34.7% (*63*). †Highest solubility.

ventral striatum (*17*, *39*). To gain deeper insight, we used five structurally distinct KOR agonists, each with distinct signaling profiles and in vivo behavioral responses (Table 1). The unbiased PCA analysis of the phosphoproteomic experimental results revealed clustering of samples treated with U-50,488H (20 nmol) and HS665 (10 nmol) on one side and treated with 6′GNTI (30 nmol) and HS666 (30 nmol) on the other in the first component. Samples treated with RB64 (3 nmol) were clustered between these but were more similar to those treated with U-50,488H and HS665 (fig. S8). Further bioinformatic analysis showed significant enrichment for the GO annotations "potassium channel complex," "cell junction," and "excitatory synapse" (fig. S9A) (*40*) based on the sites regulated by U-50,488H, HS665, and RB64 but not by 6′GNTI and HS666. This prompted us to focus on differential phosphorylation of synaptic proteins, particularly because dynamic phosphorylation of synaptic proteins in the striatum affects synaptic plasticity (*33*) and membrane trafficking (*41*).

Overall, large-scale dynamic phosphorylation changes on synaptic proteins were present at the 5-min interval and ebbed away at the 30-min interval (fig. S9B). The most prominent dynamic phosphorylation changes mediated by U-50,488H, HS665, and RB64, but not by 6′GNTI and HS666, involved synaptic proteins associated with dopaminergic, glutamatergic, and GABAergic signaling and synaptic vesicle release. This included a down-regulation of the phosphorylation state of the *N*-methyl-D-aspartate (NMDA) receptor and many of its scaffolding proteins, dynamins (Ser^{851} on Dnm1), members of the SNARE complex, and a multitude of ion channels (Fig. 4A).

We were especially intrigued by DARPP-32, a downstream effector of dopaminergic signaling that is also regulated by glutamatergic signaling. DARPP-32 is a potent inhibitor of protein phosphatase 1 (PP1) and plays an important role in synaptic plasticity (*42*). Dynamic phosphorylation of DARPP-32 in general, and Ser^{97} specifically, is regulated by various drugs of abuse (*43*, *44*) and is correlated with nuclear accumulation of DARPP-32 and the control of gene expression related to long-term synaptic plasticity (*43*). From the MS measurements, we found Ser^{97} to be specifically dephosphorylated at 5 min after application of U-50,488H in the striatum by a factor of 2. Immunohistochemistry clearly showed this dephosphorylation in both the caudate putamen (CPu) and NAc, the two main loci of the striatum. This effect was specific to Ser^{97}, whereas Ser^{192} was not regulated (Fig. 4C).

Other interesting ligand-directed dynamic phosphorylation events include the cannabinoid receptor 1 (CB1). The phosphorylation level of CB1 at Ser^{317} was shown to correlate with CB1 activity; mounting evidence links CB1 activation with KOR activation (*45*–*47*). Our current data suggest that cross-talk between CB1 and KOR may at least be partially regulated through dynamic phosphorylation of CB1 at Ser^{317} (Fig. 4, A and C).

Among the kinases, down-regulation of Src kinase at Ser^{74} is noteworthy because of the known role of Src in phosphorylating many of the above-mentioned substrates and regulating synaptic plasticity (*48*). Other sites of interest include Ser^{7} of G protein gamma subunit 12, which is an immediate downstream effector of KOR, and Ser^{1459} of the NMDA receptor 2a subunit.

When comparing the effects of the five agonists, we observed that 6′GNTI and HS666 did not significantly regulate the abovementioned phosphosites, whereas HS665 and RB64 affected some but not all of the sites regulated by U-50,488H (Fig. 3C). This may reflect differential activation of pathways through KOR, but may also be influenced by differences in biodistribution, the applied dosage, efficacy, or pharmacokinetic or off-target effects that are undetected using our method. However, viewing the phosphoproteomic changes of synaptic proteins as a whole, U-50,488H, HS665, and RB64 exhibited greater similarity to each other than to 6′GNTI and HS666, even though each ligand induced a somewhat unique perturbation to the phosphoproteome (Fig. 3A and fig. S10). This illustrates the importance of investigating the molecular basis of in vivo GPCR signaling at the systems level instead of at the individual phosphorylation level.

These examples illustrate the complexity and subtlety of the differential regulation of various signaling pathways in the nervous systems by these two ligand classes in the important context of the synapse.

Phosphatases participate in KOR striatal U-50,488H–mediated signaling

The large-scale dephosphorylation of synaptic proteins in the striatum after 5 min of stimulation by U-50,488H but not 6′GNTI raised the question of whether they specifically activate Ser/Thr phosphatases. To test this hypothesis, we injected mice i.c. with three functionally distinct phosphatase inhibitors: fostriecin, a protein phosphatase 2A (PP2A) and protein phosphatase 4 (PP4) inhibitor; calyculin A, a PP1 and PP2A inhibitor; and tautomycetin, a selective PP1 inhibitor (Fig. 5). One hour after treatment, mice received U-50,488H; brains were dissected 5 min later, and their striatum was processed for phosphoproteomic measurements as previously described.

Consistent with our hypothesis, we found 300 phosphorylation sites in the striatum for which dephosphorylation was abolished in the presence of one or more phosphatase inhibitors. This establishes that phosphatases play an important role in U-50,488H–mediated signaling. About half of these phosphatase-sensitive sites belong to synaptic proteins, in agreement with the importance of phosphatases in synaptic functions (*49*). In addition, GO enrichment analysis of the proteins regulated by phosphatase revealed enrichment of "clathrin-dependent endocytosis,"

"synaptic vesicle priming," and "small GTPase regulator activity," which suggests that U-50,488H–mediated but not 6′GNTI-mediated pathway(s) may be involved in neurotransmitter release and membrane receptor trafficking (fig. S11).

Among the 300 phosphatase-sensitive sites, a minor cluster was insensitive to tautomycetin pretreatment (Fig. 5A). Unlike the other two inhibitors, tautomycetin selectively inhibits PP1 but not PP2A; therefore, these sites are most likely mediated by PP2A. In this group of sites, we were especially intrigued by the aforementioned phosphorylation of Ser^{317} of the CB1 receptor and Ser^{762} of the $GABA_B$ receptor (Fig. 5B), both well-known GPCRs. Thus, phosphoproteomics can reveal additional mechanistic details in the complexity of in vivo GPCR signaling through the phosphorylation of coexpressed GPCRs. Together, these results highlight the importance of phosphatases in GPCR signaling at synapses.

Conditioned place aversion, but not antinociceptive or anticonvulsant effects, is ablated by mTOR pathway blockade

The bioinformatic analysis of the sites differentially regulated by U-50,488H, HS665, and RB64 but not by 6′GNTI and HS666 also revealed that the mechanistic target of rapamycin (mTOR) signaling pathway was enriched in the striatum at the 5-min interval and in the cortex at 30 min (Fig. 6, A and B). In the striatum, mTOR was the most significantly regulated pathway, whereas in the cortex it was among the top five. This interesting finding from our unbiased phosphoproteomics approach links to previous reports of mTOR involvement in ketamine-induced and fluoxetine (Prozac)–induced antidepressant effects in a region-dependent manner (*50*, *51*) as well as dysfunction of the mTOR pathway in the prefrontal cortex of patients with major depressive disorders (*52*).

U-50,488H is well established to produce CPA in rodents (*53*, *54*). A recent report indicated that through central injection in mice, 6′GNTI did not cause CPA, although it showed robust antiseizure activity similar to U-50,488H (*7*). RB64 was also reported to produce a unique spectrum of behavioral activities, including CPA in mice (*9*). HS665 and HS666 are recently synthesized KOR-specific agonists (*55*). HS665, but not HS666, was reported to produce profound CPA (*11*) (Table 1). Combined with our present observation that only U-50,488H, HS665, and RB64, but not 6′GNTI and HS666, induce mTOR signaling, this led us to hypothesize that pretreating mice with an mTOR inhibitor could abolish the aversive behavior induced by U-50,488H.

We investigated the effects of pretreatment with temsirolimus, an mTOR inhibitor, at a dose of 8 mg/kg. Mice were pretreated for 1 hour with temsirolimus, saline, or vehicle controls before receiving U-50,488H or saline injection for each conditioning session (Fig. 6C). As expected, treatment with U-50,488H induced a highly significant response in the CPA assay, consistent with previous findings that this KOR agonist induced aversive effects in mice. Pretreatment with the mTOR inhibitor abolished the CPA induced by U-50,488H alone (Fig. 6C). This shows that mTOR blockade indeed suppressed the aversive effects linked to KOR activation, which is in agreement with our hypothesis. The anticonvulsive effect of U-50,488H as assessed in the pentylenetetrazole (PTZ) (tail vein infusion)–induced seizure model (Fig. 6D) and the antinociceptive effect assessed in the acetic acid–induced writhing test (Fig. 6E) were unaffected by mTOR inhibition.

Probing the downstream molecular mechanism of mTOR activation, we found that U-50,488H, HS665, and RB64 on one hand and 6′GNTI and HS666 on the other differentially regulated phosphorylation sites of proteins involved in translation, including Eif4b (Ser^{504}) and Rps6 (Ser^{240}, Ser^{244}) (fig. S12). Both proteins are part of the mTOR signaling pathway, and their phosphorylation sites are regulated by the kinases involved in the same pathway. A body of evidence already links mTOR-mediated alteration of protein synthesis with synaptic plasticity, learning, and memory, specifically through long-term potentiation and depression (*56*). Our present data specifically connect KOR activation to depressive/aversive behavior involving the activation of mTOR, possibly through its effect on protein translation; hence, this connection can be pharmacologically separated.

To investigate the upstream mechanism that activates mTOR, we used the neuroblastoma cell line (Neuro 2A) with stable expression of mouse KOR. Cells were pretreated with vehicle or pertussis toxin (PTX) (200 ng/ml), a specific inhibitor of the $G_{i/o}$ signaling pathway, for 2 hours, followed by vehicle or U-50,488H (10 μM) for 30 min. Phosphoproteomic analysis of these cells revealed that mTOR signaling was the most enriched pathway in cells treated with U-50,488H or with U-50,488H + PTX ($P < 10^{-8}$) but not in cells treated with PTX alone, indicating that mTOR signaling is activated in a G protein–independent manner (fig. S13). Specifically, we discovered that Ser^{939} of Tsc2 was phosphorylated by U-50,488H treatment in a PTX-insensitive manner (fig. S14). Phosphorylation of Tsc2 by Akt modulates mTOR signaling (*57*), and we found an additional group

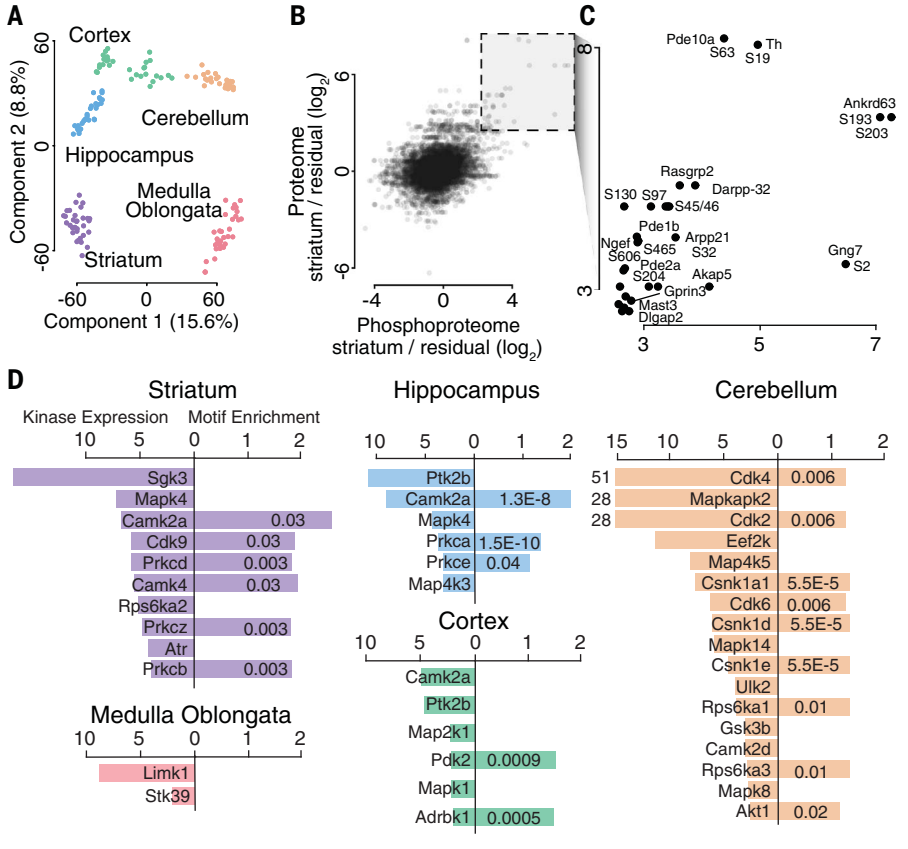

Fig. 2. Unstimulated brain phosphoproteomic architecture. (**A**) Principal components analysis (PCA) of all brain samples. The first and second components are shown. (**B**) Welch *t* test difference between striatum and rest of brain (residual) at the phosphoproteomic level (*x* axis) and the proteomic level (*y* axis); Pearson correlation = 0.53. (**C**) Zoom-in of plot in (B) for proteins that are highly expressed in the striatum. (**D**) Differential kinase expression in each region in comparison to residual (left) and motif enrichment (right) of the same kinase, when the motif is available. The motif enrichment is the result of the Fisher exact test on phosphosites that exhibit high intensity in each region relative to the residual. The number on each bar indicates the *P* value of the enrichment.

of Akt substrates to be influenced by U-50,488H that were also PTX-insensitive (fig. S15) among molecules that likely mediate G protein–independent signaling. Akt was previously discovered to be downstream of KOR activation in the cultured primary striatal neurons (*18*), indicating that Akt activation might be an interesting line of research to pursue.

Along with the mTOR pathway, we also found the mitogen-activated protein kinase (MAPK) pathway to be enriched in U-50,488H and U-50,488H + PTX stimulated Neuro 2A cells. Early activators such as Sos1 and Raf1 were dephosphorylated in a PTX-insensitive manner (fig. S14). Activation of the MAPK pathway has already been linked to KOR G protein–independent signaling pathways and KOR-mediated aversion (*16*, *17*). Thus, our current data establish that both mTOR and the MAPK pathways are activated in a G protein–independent manner. This leads us to speculate that these two G protein–independent signaling pathways are activated in a similar fashion to activation downstream of the insulin receptor: MAPK through the Grb2-Sos1-Raf branch, and mTOR activation through the Akt-Tsc2 branch (fig. S14).

Discussion

This study offers a systems view of in vivo brain GPCR signaling. Even though specifically KOR-mediated signals derive from interaction of ligands with the same GPCR, signaling pathways are channeled toward distinct physiological effectors in each brain region and at each time point. We found that the basal phosphoproteome in different regions correlates with the abundance of the proteome and the kinome. This was not the case for the regulated phosphoproteome, reflecting the importance of additional factors such as protein interaction networks, neuron-neuron contacts, and brain circuitry in the makeup of the regulated phosphoproteome. This was apparent from signaling propagation to brain areas with minimal KOR expression at later time points. Such results emphasize that a more complex concept of GPCR signaling, which accounts for diversity of cell types and cell-cell communication in addition to in vitro concepts such as functional selectivity, is necessary for a better understanding of the subtleties of in vivo GPCR signaling.

Our study has also established that the phosphoproteomic approach could disentangle beneficial antinociceptive and anticonvulsant effects from unwanted KOR-mediated side effects such as aversion at the pathway level, and possibly could use this knowledge to separate one from the other. This in vivo approach bypasses the need of in vitro characterization of ligands and minimizes the risk associated with in vitro–in vivo translation. Although temsirolimus, the mTOR inhibitor used here, is an FDA-approved chemotherapy agent, clinical application of these results would likely require a specific modulation of the mTOR network that results in the desired behavioral outcomes.

We propose phosphoproteomics combined with pharmacological tools and behavioral assessments as a general approach for studying GPCR signaling in vivo. Together with appropriate in vitro cellular systems, detailed molecular mechanisms of individual pathways can be characterized, leading to a more rational approach for GPCR drug discovery. Our approach bridges in vitro–based and purely behavioral studies, offering the opportunity to discover, without a priori assumptions, signaling pathways that can be pharmacologically manipulated to achieve specific therapeutic benefits.

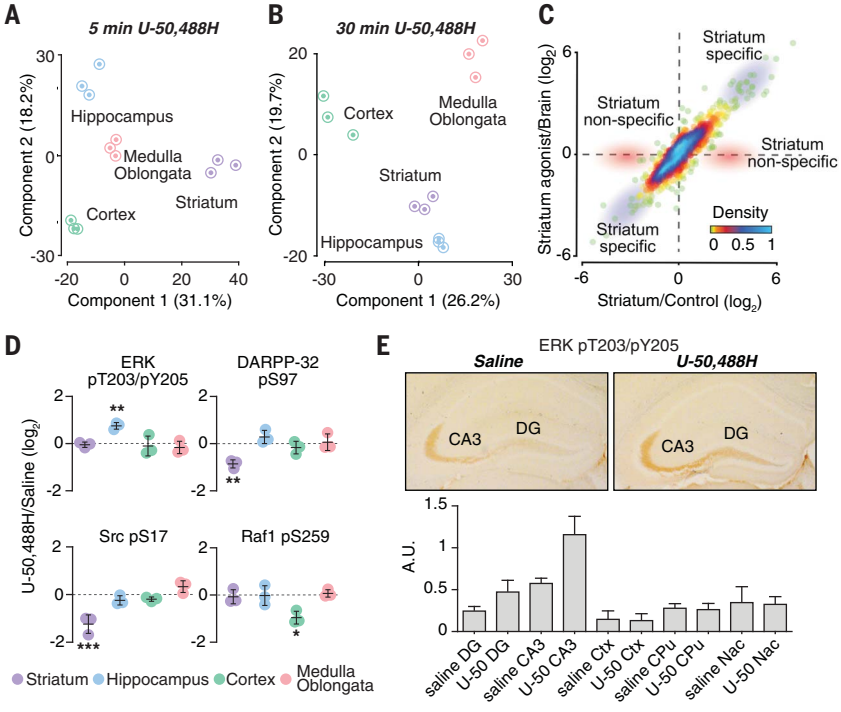

Fig. 3. Region-specific outcomes of U-50,488H–induced activation of KOR. (**A**) PCA of normalized spatial and temporal U-50,488H–regulated sites (significant by ANOVA) versus their respective saline controls at the 5-min time point. (**B**) Same as (A) at the 30-min time point. (**C**) Scatterplot showing striatum-specific U-50,488H signaling. The *x* axis denotes the $\log_2$ intensity difference of striatum samples between U-50,488H and saline control; the *y* axis denotes the $\log_2$ intensity difference between all the striatum samples and those from the other brain regions. U-50,488H–regulated sites that are striatum-specific fall on the diagonal, as indicated by the area shaded in blue; U-50,488H–regulated sites that are in common among all brain regions fall on the *x* axis, as indicated by the area shaded in red. (**D**) Quantification of selected sites in four brain regions. The *y* axis denotes the $\log_2$ intensity difference between U-50,488H and saline samples in the respective regions. Error bars represent mean ± SD. (**E**) Immunohistochemistry of ERK pT203/pY205. Top: Representative images of stained hippocampus with saline or U-50,488H treatment; specific regions in hippocampus are indicated within the images (n = 4 per group). Bottom: Histogram showing quantification of ERK pT203/pY205 immunoreactivity in various regions including the hippocampus. CA3, cornu ammonis field 3; Ctx, cortex; CPu, caudate putamen (a subregion of striatum); DG, dentate gyrus; NAc, nucleus accumbens (a subregion of striatum). Error bars represent mean ± SD (n = 4). Data in (C) to (E) were collected 5 min after injection. A.U., arbitrary units.

Materials and methods

Animals

All animal care and experimental procedures were approved by the Austrian Animal Experimentation Ethics Board in compliance with the European Convention for the Protection of Vertebrate Animals Used for Experimental and Other Scientific Purposes ETS no. 123.

We investigated prodynorphin knockout (pDyn-KO) and KOR knockout (KOR-KO) mice (male, adult) in the phosphoproteomic and most behavioral studies. CD1 mice (male, adult) were used in the writhing test. pDyn-KO mice (*58*) and KOR-KO mice (*59*) were backcrossed onto the C57BL/6N background over 10 generations. For breeding and maintenance, mice were group housed (maximum of five animals per cage) with free access to food and water. Temperature was fixed at 23°C and 60% humidity with a 12-hour light-dark cycle (lights on 7 a.m. to 7 p.m.). Mice of the same strain and age were arbitrarily sorted into groups, splitting litters into different groups. For the animal experiments, the experimenter was blinded to the treatments of the animals.

Phosphoproteomic experiments were carried out in pDyn-KO mice to minimize the influence of endogenous dynorphins. Endogenous dynorphins are released under stressful situations such as handling. They are considered unbiased full agonists and their release during the treatment

is likely to influence the phosphorylation profile especially of biased, partial agonists. Indeed, comparing the profiles of 6′GNTI on wild-type and pDyn-KO mice resulted in comparable, yet less reproducible, phosphorylation patterns.

KOR agonists

We investigated five KOR ligands: U-50,488H, HS665, RB64, 6′GNTI, and HS666. An overview of their in vitro pharmacological profiles and behavioral effects is presented in Table 1. 6′GNTI, generated in the laboratory of P. Portoghese, is used as tool ligand to study KOR pharmacology in vitro and in vivo. It was demonstrated to produce antinociception in mice after central intrathecal administration (*46*) and anticonvulsant effects without inducing conditioned place aversion after central i.c. administration in mice (*7*). HS665 and HS666 are structurally distinct KOR ligands from the class of diphenethylamines from the laboratory of H. Schmidhammer, displaying interesting pharmacological profiles (*11*, *40*, *60*). HS665 is a potent, selective, and full agonist for KOR G protein activation. It produces antinociception and CPA in mice (*61*, *62*). HS666 is a selective KOR partial agonist (*11*). RB64 was generated in the laboratory of B. Roth as an analog of salvinorin A. As a KOR full agonist, RB64 was established to have a unique spectrum of activities in vivo by producing analgesia (without causing sedation) and CPA in mice (*9*). All compounds were applied dissolved in saline at the relevant concentration except of RB64, which was only soluble in saline containing 10% dimethyl sulfoxide (DMSO).

In phosphoproteomic experiments, KOR ligands (U-50,488H, 20 nmol; 6′GNTI, 30 nmol; HS665, 10 nmol; HS666, 30 nmol; RB64, 3 nmol) were injected i.c. into pDyn-KO mice under mild (2%) sevofluorane anesthesia in a fixed volume of 3 µl. Each experimental group included three mice. After 5 or 30 min, animals were killed by cervical displacement; the brain was removed from the skull and microdissected immediately. The hippocampus, striatum, cortex, cerebellum, medulla oblongata, and olfactory bulbs were flash-frozen in liquid nitrogen at 2:15, 3:05, 3:30, 3:50, 4:10, and 5:00 min after decapitation. Central application of drugs avoids several pharmacokinetic effects and therefore is considered to yield better comparability. Moreover, 6′GNTI does not permeate the blood brain barrier in sufficient amounts. U-50,488H was purchased from Tocris; 6′GNTI was a gift from the NIDA Drug Supply Program; HS665 and HS666 were synthesized according to the published procedure (*61*); and RB64 was a generous gift from B. Roth laboratory.

Phosphatase inhibitors

The phosphatase inhibitors tautomycetin (0.05 mg/kg), fostriecin (0.05 mg/kg), and calyculin (0.01 mg/kg) (all from Tocris) were applied intraperitoneally (i.p.) 1 hour before KOR agonists. All of these phosphatase inhibitors are soluble in saline at the dosage applied.

Pertussis toxin and Neuro 2A cells

FmK6H-N2A cells were subcultured in a 100-mm plate in complete medium [GIBCO 41500-034, minimum essential medium supplemented with 10% fetal bovine serum and blasticidin (1 µg/ml)] and allowed to grow to 80% confluency (~8×10^6 cells) in a CO_2 incubator. The cells were washed and incubated with serum-free medium for 1 hour. The pertussis toxin (PTX, List Biological Laboratories Inc., Campbell, CA) was added to the cell medium at 0.2 µg/ml and allowed reaction for 1 hour in the incubator. The cells were then

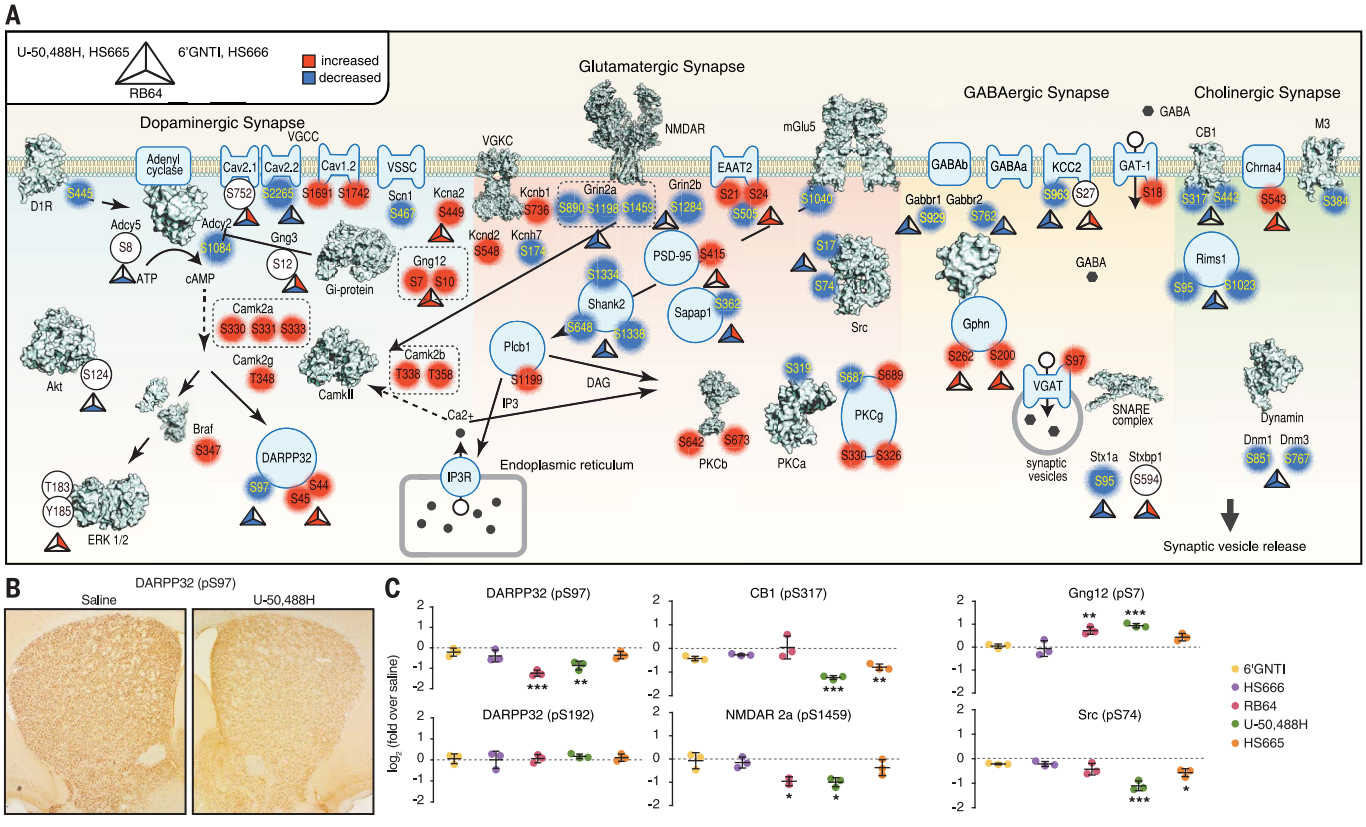

Fig. 4. KOR-mediated signaling at synapses after 5 min. (**A**) Proteins assigned to different KEGG pathways, with particular phosphosites of each protein indicated by the position of the site in a circle. Empty, red, and blue circles indicate no change, increase, and decrease of phosphorylation by U-50,488H stimulation, respectively. Significant U-50,488H–altered sites are chosen from the pairwise Welch *t* test between U-50,488H and saline samples, with cutoff of $P < 0.05$ and difference of >70% in each direction. Triangles next to the circles indicate changes of phosphorylation mediated by three different groups of KOR agonists according to their bioinformatics clustering (fig. S8). The coloring is the same as above. (**B**) Immunohistochemistry in a coronal section of striatum using an antibody to DARPP-32 p97, showing decreased immunoreactivity by U-50,488H treatment ($n = 4$ per group). (**C**) Quantification of selected phosphosites from (A). Samples were analyzed by ANOVA post hoc Dunnett test. *$P < 0.05$, **$P < 0.01$, ***$P < 0.001$ versus saline (control) group. Error bars represent mean ± SD ($n = 3$).

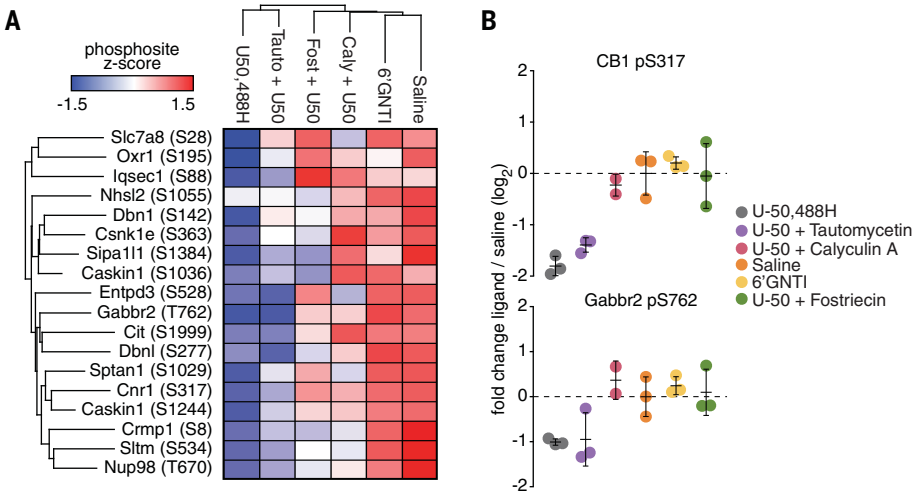

Fig. 5. PP2A mediates U-50,488H actions. (**A**) Heat map of the hierarchical clustering results of U-50,488H–induced changes in PP2A substrates. These sites are dephosphorylated after U-50,488H application with or without tautomycetin (Tauto) pretreatment (PP1-specific inhibitor). But they are not affected by 6′GNTI or by pretreatment with the PP2A inhibitors fostriecin (Fost) or calyculin (Caly) combined with U-50,488H stimulation. The median intensity of three biological replicates in each condition was *z*-scored and colored as shown in the scale bar. (**B**) Selected sites from (A). The *y* axis is the $\log_2$ difference between each condition and saline control. Error bars represent mean ± SD (n = 3).

further treated for 30 min with 10 μM U-50,488H or vehicle. The cells were quickly washed with PBS buffer, collected in PBS containing 1 mM EDTA, and centrifuged. The cell pellets were immediately dissolved in sample buffer (4% SDS, 50 mM Tris, pH 7.4) with the aid of three short bursts of sonication. Samples were then stored at −80°C for subsequent phosphoproteomic analysis.

Phosphoproteomic sample preparation

Frozen brain tissues were transferred into "lysing matrix D" tubes, which contained 1.4-mm ceramic beads (MP Biomedicals) with 400 μl of lysis buffer (100 mM Tris pH 8.5, 4% SDS). Samples were then lysed using Fastprep 24 (MP Biomedicals) at 4 m/s. Samples were then spun down at the maximum speed for 90 min. Frozen cell samples were processed in the same lysis buffer.

After heating for 10 min at 95°C, cold acetone was added to each tube to induce protein precipitation to reach 4:1 (acetone: sample v/v). Protein precipitates were redissolved into 500 μl of the resuspension buffer [100 mM ammonium bicarbonate (ABC), 100 mM Tris pH 8.5, 10% 2,2,2-trifluoroethanol (TFE), 10 mM tris (2-carboxyehtyl)phosphine (TCEP), 40 mM 2-choloroacetamide (CAA)]. After incubation at 50°C for 10 min, samples were transferred into a 96–deep well plate (DWP), from which the protein concentration was determined using the BCA assay. From then on, all the following steps were performed in parallel. The EasyPhos protocol was applied to the samples as described (*30*). Briefly, samples were treated with trypsin and LysC at 100:1 (protein:enzyme w/w) with agitation (2000 rpm) at 37°C; 150 μl of 3.2 M KCl, 55 μl of 150 mM KH_2PO_4, 800 μl of acetonitrile (ACN), and 95 μl of trifluoroacetic acid (TFA) were added to each sample. Digested peptides were enriched with TiO_2 beads (10:1 beads:protein w/w) at 40°C for 5 min at 2000 rpm. Afterward, the phosphopeptide-containing TiO_2 beads were further washed with 4 ml of wash buffer (60% ACN, 1% TFA) and treated with elution buffer (40% ACN, 15% NH_4OH). Eluted phosphopeptides were concentrated in a SpeedVac for 15 min at 45°C; during this process, volatile chemicals such as NH_4OH and ABC were removed. Samples were then desalted using StageTips packed with SDB-RPS membranes and then concentrated in a SpeedVac until dry. A 6-μl volume of MS loading buffer (2% ACN, 0.3% TFA) was added to the samples, which were then sonicated for 5 min in a water bath sonicator.

High-performance liquid chromatography and MS measurements

Samples were loaded onto 50-cm columns packed in-house with C18 1.9 μM ReproSil particles (Dr. Maisch GmbH), with an EASY-nLC 1000 system (Thermo Fisher Scientific) coupled to the MS (Q Exactive HF, Thermo Fisher Scientific). A homemade column oven maintained column temperature at 50°C. Peptides were introduced onto the column with buffer A (0.1% formic acid) and eluted with a 140-min gradient of 5 to 25% of buffer B (60% ACN, 0.1% formic acid), both at a flow rate of 300 nl/min.

A data-dependent acquisition (TopN) MS method was used, in which one full scan (300 to 1600 m/z, R = 60,000 at 200 m/z) at a target of 3×10^6 ions was first performed, followed by 10 data-dependent MS/MS scans with higher-energy collisional dissociation [target 10^5 ions, max ion fill time 120 ms, isolation window 1.6 m/z, normalized collision energy 27%, underfill ratio 40%, R = 15,000 at 200 m/z]. Dynamic exclusion of 60 s and apex trigger (4 to 7 s) were enabled.

Bioinformatic workflow and data analysis

The raw MS spectra were processed using MaxQuant version 1.5.5.2 (*61*). We applied a false discovery rate (FDR) < 0.01 at the level of peptide-spectrum matching, protein assembly, and modifications identification. We estimated protein, peptide, and site FDR using a target-decoy approach with the reverse sequence database. This step was performed in the Andromeda search engine (*62*) integrated in the MaxQuant environment. Searches were performed using the Mouse UniProt FASTA database (September 2014). In addition to the default settings, phospho (STY) was selected as a "variable modification" to enable the identification of peptides containing phosphorylated Ser, Thr, or Tyr residues. The "match between runs" (MBR) feature was enabled, with a matching time window of 1 min.

Further bioinformatics analysis was conducted in Perseus (version 1.5.2.17) (*63*), Microsoft Excel, and R statistical computing software. Annotations were extracted from Gene Ontology (GO) (*64*) and the Kyoto Encyclopedia of Genes and Genomes (KEGG). The synaptic proteins were annotated according to the synaptome database (http://metamoodics.org/SynaptomeDB/) (*65*). Kinase-substrate relationships were based on the phosphositeplus database (phosphosite.org) (*66*). Interaction network analysis was performed with the web-based string database (string-db.org), using the active data source of "Experiments" and "Database" and the biogrid interaction data depository (https://thebiogrid.org/). Cytoscape (version 3.3.0) and its plugin jActiveModules were used to analyze the architecture of subnetworks and to visualize the interaction data (*67*); t tests were conducted using the Welch t-test formula implemented into the Perseus environment unless stated otherwise. Multiple sample comparison was performed using ANOVA with post hoc Dunnett test and the "multicomp" package in R.

For convenience of data handling, all samples were first transformed into a $\log_2$ scale and data normalization was performed. Briefly, after valid value filtering, a median subtract was performed. This is based on the assumption that the majority of the phosphoproteome is unperturbed by the ligand stimulation. In cases where a batch effect was observed (e.g., when experiments were measured in separate MS sessions), normalization by PCA component subtraction was performed. The component in PCA that was correlated with the batch effect was removed by multiplying each sample by its own normalization factor.

To alleviate the "missing value" problem, we performed stringent valid value filtering requiring at least 30% of valid values in all groups, at least 70% of valid values in at least one group, and 50% valid values across all samples. In addition, we removed any columns where quantified values were fewer than 10% of the mean

valid values within the group. In each brain region, we usually encountered 11,000+ sites after this stringent filtering. When comparing the phosphoproteome across regions, we quantified 6000 to 7000 sites after filtering. For most of the analysis, whenever possible we did not perform imputation. If necessary, we imputed the missing values from a random Gaussian-shaped distribution applying a downshift of 1.5 times the standard deviation of the global dataset, and a width of 0.5 times the standard deviation. This effectively simulated values toward the lower end of the intensity distribution, as expected.

PCA, a hybrid hierarchical *k*-means clustering algorithm, and categorical enrichment tests (Fisher exact test) were performed in the Perseus environment. The detailed description can be found in (*63*). The PCA analysis was performed on the basis of singular value decomposition. The categorical enrichment tests were performed in the following steps: We first performed ANOVA on samples from one region and time point (background) using a post hoc Dunnett test. To ensure the simplicity of the test, we pooled U-50,488H, HS665, and RB64 into one group and 6′GNTI and HS666 into another. We then selected groups of phosphosites that passed a threshold of $P < 0.05$ for the former but $P > 0.05$ for the latter. A Fisher exact test was used to test categorical enrichment of the above-mentioned phosphosites using the "background" mentioned above. The ANOVA post hoc Dunnett test was performed for phosphoproteomic analysis using R.

Interaction network analysis

Interaction network analysis was performed using pairwise Welch *t* tests (for example, between U-50,488H and saline samples) to determine U-50,488H–regulated sites in each brain region after 5 min of stimulation. Proteins carrying significantly regulated phosphorylation sites were subsequently used as input for interaction analysis using the String database and Cytoscape plugin "jActiveModule" (*67*). In the jActiveModule analysis, the Biogrid mouse interaction network was also used as an input. The jActiveModule analysis was originally designed to find the highly connected modules or subnetworks, which exhibit similar responses to an experimental condition. We further designated the response as changes in the phosphorylation level in our experiments. The consensus networks between these two approaches in each brain region were selected and displayed.

Categorical enrichment analysis

A Fisher exact test was performed to reveal annotations and pathways that are significantly enriched in the regulated group for each brain region. The output of this test is a *P* value (indicating a degree of significance) and an enrichment factor (indicating the level of enrichment with respect to the background).

The "annotation matrix" algorithm described previously (*36*) was also used to identify cellular mechanisms and processes proteins harboring large-scale dynamic phosphorylation alterations. We reasoned that multiple dynamic phosphorylation perturbation on proteins that belong to the same cellular mechanism are likely to occur if the pathway is recruited. Therefore, we performed nonparametric Mann-Whitney *U* tests between phosphosites carrying the same annotation against the background.

Immunohistochemistry

Immunohistochemistry was performed as described (*68*). Briefly, mice were anesthetized with thiopental (150 mg/kg i.p.). As soon as they fell asleep (~1 min after injection), drugs were injected intracisternally and mice were perfused 5 min after drug treatment with 4% paraformaldehyde in PBS (50 mM phosphate-buffered saline, pH 7.2). Immunohistochemistry was performed on coronal 40-μm vibratome sections incubated free-floating in blocking solution (10% normal goat serum and 0.3% Triton X-100 in TBS) for 90 min. Primary antibodies against pDARPP-32 (1:400; Cell Signaling Technology,

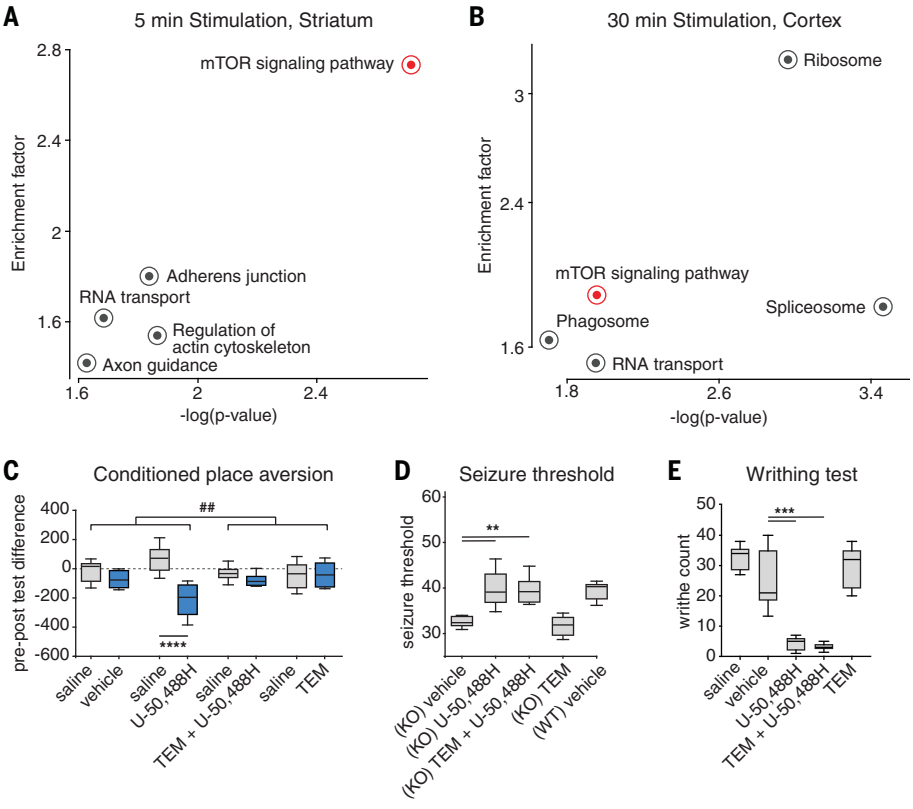

Fig. 6. Blockade of mTOR signaling inhibits conditioned place aversion but does not influence anticonvulsant or antinociceptive effects. (**A**) Fisher exact test on the group of sites that are significantly regulated only by U-50,488H and HS665 in the striatum after 5 min of KOR activation. (**B**) Same as (A) but in cortex after 30 min of stimulation. The *x* axis is the negative log of the *P* value obtained from the Fisher exact test; the *y* axis is the relative difference between the percentages of significantly differentially regulated sites that carried the depicted annotations over the percentage of all sites that carried the same annotation. (**C**) Conditioned place aversion in pDyn-KO mice (U-50,488H, 2.5 mg/kg; $n = 6$ to 8 per group). Three-way ANOVA with post hoc Šidák correction for multiple comparison was performed with time spent in each chamber as the first factor, treatment of U-50,488H as the second factor, and treatment of temsirolimus (TEM) as the third factor. The interaction term between the first factor and TEM yields $P = 0.0074$, whereas TEM alone does not induce significant changes, demonstrating that TEM treatment has a highly significant effect on U-50,488H–mediated aversion. The results of post hoc comparison between time spent in each chamber is indicated. $^{****}P < 0.0001$, $^{\#\#}P < 0.01$. (**D**) PTZ-induced seizure threshold in pDyn-KO mice (U-50,488H, 20 mg/kg; $n = 5$ per group). KO, pDyn-KO; WT, wild type. Two-way ANOVA with post hoc Dunnett multiple-comparisons test and vehicle as control was performed with treatment of U-50,488H as the first factor and treatment of TEM as the second factor. U-50,488H treatment was significant ($P < 0.0001$), but treatment of TEM was not significant ($P = 0.5809$). Post hoc Dunnett multiple-comparisons tests are shown. $^{**}P < 0.01$. (**E**) Writhing test in CD1 mice (U-50,488H, 2 mg/kg; $n = 6$ per group). A two-tailed *t* test showed no significant difference between saline and vehicle. Two-way ANOVA with post hoc Dunnett multiple-comparisons test and vehicle as control was performed with the same factors as in (D). U-50,488H treatment was significant ($P < 0.0001$); treatment of TEM was not ($P = 0.7627$). Post hoc Dunnett multiple-comparisons tests are shown. $^{***}P < 0.001$. Bars represent mean ± SEM.

#D11A5) or pERK, (1:400; Cell Signaling Technology, #9101) were applied overnight at room temperature followed by horseradish peroxidase–conjugated secondary antibodies (1:500, Dako) and 3,3′-diaminobenzidine for detection.

Animal behavioral experiments

Drug preparation

U-50,488H was dissolved in sterile physiological saline (0.9%). Temsirolismus (Tocris) was prepared in 10% DMSO and 3% Tween 20 in sterile physiological saline (0.9%). Vehicle (10% DMSO and 3% Tween 20 in physiological saline) or test compounds were administered in a volume of 10 μl per 1 g body weight.

Conditioned place avoidance

The conditioned place avoidance (CPA) tests were conducted in pDyn-KO mice using a custom-made, three-chamber apparatus (*69*). The conditioning procedure comprised a pretest session, four consecutive training days [two training sessions per day, one each for drug (afternoon) or saline (morning) with a minimum interval of 4 hours], and a CPA test on day 6. Pretest and CPA test session lengths were 15 min, and the conditioning sessions lasted 30 min (*7*). Drugs were assigned to the chambers in an unbiased design. For conditioning, all mice received vehicle 60 min before saline in the morning. In the afternoon, two groups of mice received temsirolimus (8 mg/kg in vehicle) 60 min before injection of either U-50,488H (2.5 mg/kg) or saline. Two other groups received vehicle 60 min before injection of either U-50,488H (2.5 mg/kg) or saline. The difference in time spent in the drug-paired versus the saline-paired box before and after conditioning was evaluated. Each experimental group included six to eight animals.

Pentylenetetrazole-induced seizures

A threshold for pentylenetetrazole (PTZ)–induced seizures was measured through infusion of PTZ (10 mg/ml in saline) through the tail vein in freely moving pDyn-KO mice as described (*7*). Animals were pretreated with either vehicle or temsirolimus (8 mg/kg i.p.) 60 min before PTZ infusion and with saline or U-50,488H (20 mg/kg i.p.) 30 min before PTZ infusion. Infusion was stopped at the first appearance of tonic-clonic seizures. Threshold was calculated from volume injected and body weight (*7*). Each experimental group included five animals.

Writhing test

Writhing was induced in CD1 mice by i.p. injection of a 0.6% acetic acid aqueous solution according to the described procedure (*40*). Groups of mice received saline, vehicle (10% DMSO and 3% Tween 20 in physiological saline), temsirolismus (8 mg/kg), or U-50,488H (2 mg/kg) alone or together with temsirolismus (8 mg/kg). Drugs or controls were administered s.c. to mice; 5 min before testing (25 min after drug or controls), each animal received i.p. acetic acid solution. Temsirolismus was administered 1 hour before U-50,488H. Each mouse was placed in individual transparent Plexiglas chambers, and the number of writhes was counted during a 10-min observation period. Each experimental group included six animals.

Statistical analysis

Behavioral data were analyzed with either two-tailed *t* test or two-way ANOVA using a Dunnett test for multiple comparisons as a post hoc test (except CPA, where a three-way ANOVA with post hoc Šidák correction for multiple comparison was performed) and graphically processed with GraphPad Prism 5.0 Software (GraphPad Prism Software Inc., San Diego, CA). Data are presented as mean ± SEM, with significance set at $P < 0.05$.

REFERENCES AND NOTES

1. R. T. Dorsam, J. S. Gutkind, G-protein-coupled receptors and cancer. *Nat. Rev. Cancer* **7**, 79–94 (2007). doi: 10.1038/nrc2069; pmid: 17251915
2. L. A. Capote, R. Mendez Perez, A. Lymperopoulos, GPCR signaling and cardiac function. *Eur. J. Pharmacol.* **763** (Pt B), 143–148 (2015). doi: 10.1016/j.ejphar.2015.05.019; pmid: 25981298
3. K. Szafran *et al*., Potential role of G protein-coupled receptor (GPCR) heterodimerization in neuropsychiatric disorders: A focus on depression. *Pharmacol. Rep.* **65**, 1498–1505 (2013). doi: 10.1016/S1734-1140(13)71510-X; pmid: 24552997
4. P. F. Vonvoigtlander, R. A. Lahti, J. H. Ludens, U-50,488: A selective and structurally novel non-Mu (kappa) opioid agonist. *J. Pharmacol. Exp. Ther.* **224**, 7–12 (1983). pmid: 6129321
5. J. Morgenweck, K. J. Frankowski, T. E. Prisinzano, J. Aubé, L. M. Bohn, Investigation of the role of βarrestin2 in kappa opioid receptor modulation in a mouse model of pruritus. *Neuropharmacology* **99**, 600–609 (2015). doi: 10.1016/j.neuropharm.2015.08.027; pmid: 26318102
6. Y. Togashi *et al*., Antipruritic activity of the kappa-opioid receptor agonist, TRK-820. *Eur. J. Pharmacol.* **435**, 259–264 (2002). doi: 10.1016/S0014-2999(01)01588-6; pmid: 11821035
7. L. Zangrandi, J. Burtscher, J. P. MacKay, W. F. Colmers, C. Schwarzer, The G-protein biased partial κ opioid receptor agonist 6′-GNTI blocks hippocampal paroxysmal discharges without inducing aversion. *Br. J. Pharmacol.* **173**, 1756–1767 (2016). doi: 10.1111/bph.13474; pmid: 26928671
8. K. M. Raehal, L. M. Bohn, β-arrestins: Regulatory role and therapeutic potential in opioid and cannabinoid receptor-mediated analgesia. *Handb. Exp. Pharmacol.* **219**, 427–443 (2014). doi: 10.1007/978-3-642-41199-1_22; pmid: 24292843
9. K. L. White *et al*., The G protein-biased κ-opioid receptor agonist RB-64 is analgesic with a unique spectrum of activities in vivo. *J. Pharmacol. Exp. Ther.* **352**, 98–109 (2015). doi: 10.1124/jpet.114.216820; pmid: 25320048
10. T. F. Brust *et al*., Biased agonists of the kappa opioid receptor suppress pain and itch without causing sedation or dysphoria. *Sci. Signal.* **9**, ra117 (2016). doi: 10.1126/scisignal.aai8441; pmid: 27899527
11. M. Spetea *et al*., Selective κ receptor partial agonist HS666 produces potent antinociception without inducing aversion after i.c.v. administration in mice. *Br. J. Pharmacol.* **174**, 2444–2456 (2017). doi: 10.1111/bph.13854; pmid: 28494108
12. S. A. Martins *et al*., Towards the miniaturization of GPCR-based live-cell screening assays. *Trends Biotechnol.* **30**, 566–574 (2012). doi: 10.1016/j.tibtech.2012.07.004; pmid: 22921755
13. R. Schröder *et al*., Deconvolution of complex G protein-coupled receptor signaling in live cells using dynamic mass redistribution measurements. *Nat. Biotechnol.* **28**, 943–949 (2010). doi: 10.1038/nbt.1671; pmid: 20711173
14. J. J. Liu, R. Horst, V. Katritch, R. C. Stevens, K. Wüthrich, Biased signaling pathways in β2-adrenergic receptor characterized by 19F-NMR. *Science* **335**, 1106–1110 (2012). doi: 10.1126/science.1215802; pmid: 22267580
15. A. Manglik *et al*., Structure-based discovery of opioid analgesics with reduced side effects. *Nature* **537**, 185–190 (2016). doi: 10.1038/nature19112; pmid: 27533032
16. M. R. Bruchas *et al*., Stress-induced p38 mitogen-activated protein kinase activation mediates kappa-opioid-dependent dysphoria. *J. Neurosci.* **27**, 11614–11623 (2007). doi: 10.1523/JNEUROSCI.3769-07.2007; pmid: 17959804
17. J. M. Ehrich *et al*., Kappa Opioid Receptor-Induced Aversion Requires p38 MAPK Activation in VTA Dopamine Neurons. *J. Neurosci.* **35**, 12917–12931 (2015). doi: 10.1523/JNEUROSCI.2444-15.2015; pmid: 26377476
18. C. L. Schmid *et al*., Functional selectivity of 6′-guanidinonaltrindole (6′-GNTI) at κ-opioid receptors in striatal neurons. *J. Biol. Chem.* **288**, 22387–22398 (2013). doi: 10.1074/jbc.M113.476234; pmid: 23775075
19. L. M. Bohn, M. J. Lohse, M. N. Nitabach, P. H. Taghert, M. J. Smit, Exploring the Biology of G Protein-Coupled Receptors from In Vitro to In Vivo. *Mol. Pharmacol.* **88**, 534–535 (2015). doi: 10.1124/mol.115.100750; pmid: 26162863
20. S. M. Spangler, M. R. Bruchas, Optogenetic approaches for dissecting neuromodulation and GPCR signaling in neural circuits. *Curr. Opin. Pharmacol.* **32**, 56–70 (2017). doi: 10.1016/j.coph.2016.11.001; pmid: 27875804
21. R. Aebersold, M. Mann, Mass-spectrometric exploration of proteome structure and function. *Nature* **537**, 347–355 (2016). doi: 10.1038/nature19949; pmid: 27629641
22. N. M. Riley, J. J. Coon, Phosphoproteomics in the Age of Rapid and Deep Proteome Profiling. *Anal. Chem.* **88**, 74–94 (2016). doi: 10.1021/acs.analchem.5b04123; pmid: 26539879
23. K. Sharma *et al*., Ultradeep human phosphoproteome reveals a distinct regulatory nature of Tyr and Ser/Thr-based signaling. *Cell Rep.* **8**, 1583–1594 (2014). doi: 10.1016/j.celrep.2014.07.036; pmid: 25159151
24. A. F. Altelaar, J. Munoz, A. J. Heck, Next-generation proteomics: Towards an integrative view of proteome dynamics. *Nat. Rev. Genet.* **14**, 35–48 (2013). doi: 10.1038/nrg3356; pmid: 23207911
25. K. N. Nobles *et al*., Distinct phosphorylation sites on the β2-adrenergic receptor establish a barcode that encodes differential functions of β-arrestin. *Sci. Signal.* **4**, ra51 (2011). doi: 10.1126/scisignal.2001707; pmid: 21868357
26. G. L. Christensen *et al*., Quantitative phosphoproteomics dissection of seven-transmembrane receptor signaling using full and biased agonists. *Mol. Cell. Proteomics* **9**, 1540–1553 (2010). doi: 10.1074/mcp.M900550-MCP200; pmid: 20363803
27. K. Xiao *et al*., Global phosphorylation analysis of beta-arrestin-mediated signaling downstream of a seven transmembrane receptor (7TMR). *Proc. Natl. Acad. Sci. U.S.A.* **107**, 15299–15304 (2010). doi: 10.1073/pnas.1008461107; pmid: 20686112
28. R. T. Kendall *et al*., The beta-arrestin pathway-selective type 1A angiotensin receptor (AT1A) agonist [Sar1,Ile4,Ile8]angiotensin II regulates a robust G protein-independent signaling network. *J. Biol. Chem.* **286**, 19880–19891 (2011). doi: 10.1074/jbc.M111.233080; pmid: 21502318
29. J. D. Hoffert *et al*., Dynamics of the G protein-coupled vasopressin V2 receptor signaling network revealed by quantitative phosphoproteomics. *Mol. Cell. Proteomics* **11**, M111 014613 (2012).
30. S. J. Humphrey, S. B. Azimifar, M. Mann, High-throughput phosphoproteomics reveals in vivo insulin signaling dynamics. *Nat. Biotechnol.* **33**, 990–995 (2015). doi: 10.1038/nbt.3327; pmid: 26280412
31. M. S. Robles, S. J. Humphrey, M. Mann, Phosphorylation Is a Central Mechanism for Circadian Control of Metabolism and Physiology. *Cell Metab.* **25**, 118–127 (2017). pmid: 27818261
32. K. Sharma *et al*., Cell type- and brain region-resolved mouse brain proteome. *Nat. Neurosci.* **18**, 1819–1831 (2015). doi: 10.1038/nn.4160; pmid: 26523646
33. H. K. Lee, Synaptic plasticity and phosphorylation. *Pharmacol. Ther.* **112**, 810–832 (2006). doi: 10.1016/j.pharmthera.2006.06.003; pmid: 16904750
34. C. Schwarzer, 30 years of dynorphins—new insights on their functions in neuropsychiatric diseases. *Pharmacol. Ther.* **123**, 353–370 (2009). doi: 10.1016/j.pharmthera.2009.05.006; pmid: 19481570
35. S. Dogra, P. N. Yadav, Biased agonism at kappa opioid receptors: Implication in pain and mood disorders. *Eur. J. Pharmacol.* **763** (Pt B), 184–190 (2015). doi: 10.1016/j.ejphar.2015.07.018; pmid: 26164787
36. S. Tyanova *et al*., Proteomic maps of breast cancer subtypes. *Nat. Commun.* **7**, 10259 (2016). doi: 10.1038/ncomms10259; pmid: 26725330
37. See "Interaction network analysis" above. String database and "jActiveModule" were used.
38. M. L. Rives, M. Rossillo, L. Y. Liu-Chen, J. A. Javitch, 6′-Guanidinonaltrindole (6′-GNTI) is a G protein-biased κ-opioid receptor agonist that inhibits arrestin recruitment.

J. Biol. Chem. **287**, 27050–27054 (2012). doi: 10.1074/jbc.C112.387332; pmid: 22736766
39. A. T. Knoll, W. A. Carlezon Jr., Dynorphin, stress, and depression. *Brain Res.* **1314**, 56–73 (2010). doi: 10.1016/j.brainres.2009.09.074; pmid: 19782055
40. See "Categorical enrichment analysis" above.
41. K. M. Turner, R. D. Burgoyne, A. Morgan, Protein phosphorylation and the regulation of synaptic membrane traffic. *Trends Neurosci.* **22**, 459–464 (1999). doi: 10.1016/S0166-2236(99)01436-8; pmid: 10481193
42. P. Calabresi *et al*., Dopamine and cAMP-regulated phosphoprotein 32 kDa controls both striatal long-term depression and long-term potentiation, opposing forms of synaptic plasticity. *J. Neurosci.* **20**, 8443–8451 (2000). doi: 10.1523/JNEUROSCI.20-22-08443.2000; pmid: 11069952
43. A. Stipanovich *et al*., A phosphatase cascade by which rewarding stimuli control nucleosomal response. *Nature* **453**, 879–884 (2008). doi: 10.1038/nature06994; pmid: 18496528
44. M. Hamada *et al*., Nicotine regulates DARPP-32 (dopamine- and cAMP-regulated phosphoprotein of 32 kDa) phosphorylation at multiple sites in neostriatal neurons. *J. Pharmacol. Exp. Ther.* **315**, 872–878 (2005). doi: 10.1124/jpet.105.090852; pmid: 16040813
45. X. Wang *et al*., CB1 receptor antagonism prevents long-term hyperexcitability after head injury by regulation of dynorphin-KOR system and mGluR5 in rat hippocampus. *Brain Res.* **1646**, 174–181 (2016). doi: 10.1016/j.brainres.2016.05.055; pmid: 27262683
46. S. P. Welch, M. Eads, Synergistic interactions of endogenous opioids and cannabinoid systems. *Brain Res.* **848**, 183–190 (1999). doi: 10.1016/S0006-8993(99)01908-3; pmid: 10612710
47. R. E. Hampson, J. Mu, S. A. Deadwyler, Cannabinoid and kappa opioid receptors reduce potassium K current via activation of Gs proteins in cultured hippocampal neurons. *J. Neurophysiol.* **84**, 2356–2364 (2000). doi: 10.1152/jn.2000.84.5.2356; pmid: 11067978
48. M. W. Salter, L. V. Kalia, Src kinases: A hub for NMDA receptor regulation. *Nat. Rev. Neurosci.* **5**, 317–328 (2004). doi: 10.1038/nrn1368; pmid: 15034556
49. D. G. Winder, J. D. Sweatt, Roles of serine/threonine phosphatases in hippocampal synaptic plasticity. *Nat. Rev. Neurosci.* **2**, 461–474 (2001). doi: 10.1038/35081514; pmid: 11433371
50. M. M. Harraz, R. Tyagi, P. Cortés, S. H. Snyder, Antidepressant action of ketamine via mTOR is mediated by inhibition of nitrergic Rheb degradation. *Mol. Psychiatry* **21**, 313–319 (2016). doi: 10.1038/mp.2015.211; pmid: 26782056
51. S. K. Hwang *et al*., Everolimus improves neuropsychiatric symptoms in a patient with tuberous sclerosis carrying a novel TSC2 mutation. *Mol. Brain* **9**, 56 (2016). doi: 10.1186/s13041-016-0222-6; pmid: 27216612
52. C. S. Jernigan *et al*., The mTOR signaling pathway in the prefrontal cortex is compromised in major depressive disorder. *Prog. Neuropsychopharmacol. Biol. Psychiatry* **35**, 1774–1779 (2011). doi: 10.1016/j.pnpbp.2011.05.010; pmid: 21635931
53. R. F. Mucha, A. Herz, Motivational properties of kappa and mu opioid receptor agonists studied with place and taste preference conditioning. *Psychopharmacology* **86**, 274–280 (1985). doi: 10.1007/BF00432213; pmid: 2994144
54. R. Bals-Kubik, A. Herz, T. S. Shippenberg, Evidence that the aversive effects of opioid antagonists and kappa-agonists are centrally mediated. *Psychopharmacology* **98**, 203–206 (1989). doi: 10.1007/BF00444692; pmid: 2569217
55. M. Spetea, I. P. Berzetei-Gurske, E. Guerrieri, H. Schmidhammer, Discovery and pharmacological evaluation of a diphenethylamine derivative (HS665), a highly potent and selective κ opioid receptor agonist. *J. Med. Chem.* **55**, 10302–10306 (2012). doi: 10.1021/jm301258w; pmid: 23134120
56. J. O. Lipton, M. Sahin, The neurology of mTOR. *Neuron* **84**, 275–291 (2014). doi: 10.1016/j.neuron.2014.09.034; pmid: 25374355
57. K. Inoki, Y. Li, T. Zhu, J. Wu, K. L. Guan, TSC2 is phosphorylated and inhibited by Akt and suppresses mTOR signalling. *Nat. Cell Biol.* **4**, 648–657 (2002). doi: 10.1038/ncb839; pmid: 12172553
58. S. Loacker, M. Sayyah, W. Wittmann, H. Herzog, C. Schwarzer, Endogenous dynorphin in epileptogenesis and epilepsy: Anticonvulsant net effect via kappa opioid receptors. *Brain* **130**, 1017–1028 (2007). doi: 10.1093/brain/awl384; pmid: 17347252
59. F. Simonin *et al*., Disruption of the kappa-opioid receptor gene in mice enhances sensitivity to chemical visceral pain, impairs pharmacological actions of the selective kappa-agonist U-50,488H and attenuates morphine withdrawal. *EMBO J.* **17**, 886–897 (1998). doi: 10.1093/emboj/17.4.886; pmid: 9463367
60. K. L. White *et al*., Identification of novel functionally selective κ-opioid receptor scaffolds. *Mol. Pharmacol.* **85**, 83–90 (2014). doi: 10.1124/mol.113.089649; pmid: 24113749
61. S. Tyanova, T. Temu, J. Cox, The MaxQuant computational platform for mass spectrometry-based shotgun proteomics. *Nat. Protoc.* **11**, 2301–2319 (2016). doi: 10.1038/nprot.2016.136; pmid: 27809316
62. J. Cox *et al*., Accurate proteome-wide label-free quantification by delayed normalization and maximal peptide ratio extraction, termed MaxLFQ. *Mol. Cell. Proteomics* **13**, 2513–2526 (2014). doi: 10.1074/mcp.M113.031591; pmid: 24942700
63. S. Tyanova *et al*., The Perseus computational platform for comprehensive analysis of (prote)omics data. *Nat. Methods* **13**, 731–740 (2016). doi: 10.1038/nmeth.3901; pmid: 27348712
64. M. Ashburner *et al*., Gene ontology: Tool for the unification of biology. *Nat. Genet.* **25**, 25–29 (2000). doi: 10.1038/75556; pmid: 10802651
65. M. Pirooznia *et al*., SynaptomeDB: An ontology-based knowledgebase for synaptic genes. *Bioinformatics* **28**, 897–899 (2012). doi: 10.1093/bioinformatics/bts040; pmid: 22285564
66. P. V. Hornbeck *et al*., PhosphoSitePlus: A comprehensive resource for investigating the structure and function of experimentally determined post-translational modifications in man and mouse. *Nucleic Acids Res.* **40**, D261–D270 (2012). doi: 10.1093/nar/gkr1122; pmid: 22135298
67. M. S. Cline *et al*., Integration of biological networks and gene expression data using Cytoscape. *Nat. Protoc.* **2**, 2366–2382 (2007). doi: 10.1038/nprot.2007.324; pmid: 17947979
68. C. Schwarzer, G. Sperk, C. Rauca, W. Pohle, Neuropeptide Y and somatostatin immunoreactivity in the rat hippocampus after moderate hypoxia. *Naunyn Schmiedebergs Arch. Pharmacol.* **354**, 67–71 (1996). doi: 10.1007/BF00168708; pmid: 8832590
69. K. Kummer *et al*., Conditioned place preference for social interaction in rats: Contribution of sensory components. *Front. Behav. Neurosci.* **5**, 80 (2011). pmid: 22232578
70. J. A. Vizcaíno *et al*., 2016 update of the PRIDE database and its related tools. *Nucleic Acids Res.* **44**, D447–D456 (2016). doi: 10.1093/nar/gkv1145; pmid: 26527722
71. J. Zhu *et al*., Cloning of a human kappa opioid receptor from the brain. *Life Sci.* **56**, PL201–PL207 (1995). doi: 10.1016/0024-3205(94)00507-0; pmid: 7869844
72. S. K. Sharma, R. M. Jones, T. G. Metzger, D. M. Ferguson, P. S. Portoghese, Transformation of a kappa-opioid receptor antagonist to a kappa-agonist by transfer of a guanidinium group from the 5'- to 6'-position of naltrindole. *J. Med. Chem.* **44**, 2073–2079 (2001). doi: 10.1021/jm010095v; pmid: 11405645
73. M. Waldhoer *et al*., A heterodimer-selective agonist shows in vivo relevance of G protein-coupled receptor dimers. *Proc. Natl. Acad. Sci. U.S.A.* **102**, 9050–9055 (2005). doi: 10.1073/pnas.0501112102; pmid: 15932946
74. F. Yan *et al*., Structure-based design, synthesis, and biochemical and pharmacological characterization of novel salvinorin A analogues as active state probes of the kappa-opioid receptor. *Biochemistry* **48**, 6898–6908 (2009). doi: 10.1021/bi900605n; pmid: 19555087
75. F. Erli *et al*., Highly Potent and Selective New Diphenethylamines Interacting with the κ-Opioid Receptor: Synthesis, Pharmacology, and Structure-Activity Relationships. *J. Med. Chem.* **60**, 7579–7590 (2017). doi: 10.1021/acs.jmedchem.7b00981; pmid: 28825813

ACKNOWLEDGMENTS

We thank B. Roth and D. Itzhak for their critical and helpful comments; G. Sowa, I. Paron, and K. Mayr for expert assistance with the MS measurement; and J. Rudolph, S. Tyanova, and G. Borner for valuable advice on bioinformatics analysis. 6′-GNTI was provided by the NIDA drug supply program to C.S. RB-64 was a generous gift from B. Roth. **Funding:** Supported by the Max Planck Society for the Advancement of Science; an EMBO long-term fellowship and the Max Planck Institute stipend program (J.J.L.); Austrian Research Fund (FWF) grants I-977-B24, P-30430-BBL, and W-1206-B05 (C.S.); and NIH grants DA013429, DA041359, and AT006899 (L.-Y.L.-C.). **Author contributions:** J.J.L., C.S., L.-Y.L.-C., and M.M. initiated the project; J.J.L., C.S., and M.S. designed experiments; L.Z. and C.S. performed mice ligand injection and dissections, supervised by C.S.; J.J.L. performed sample preparation and mass spectrometry experiments with help from S.J.H.; J.J.L. performed bioinformatic analysis with help from K.S.; C.C. and Y.C. performed the PTX experiments supervised by L.-Y.L.-C.; C.S. supervised and performed phosphatase inhibitor experiments, immunohistochemistry, conditioned place aversion, and PTZ-induced seizure experiments; M.S. provided HS665 and HS666 and performed the writhing test; M.M. supervised the mass spectrometry experiments and data analysis; J.J.L., C.S., M.S., and M.M. wrote the manuscript with editing and input from K.S., S.H., M.S., and L.-Y.L.-C.; and the project was conceived by J.J.L., C.S., and L.-Y.L.-C. The mTOR behavioral response was first discovered by L.-Y.L.-C. and reproduced by C.S. **Data and materials availability:** Mass spectrometry–based proteomics data have been deposited to the ProteomeXchange Consortium via the PRIDE (*70*) partner repository with the dataset identifier PXD006637. N2A-FmK6H cells are available from L.-Y.L.-C. under a material transfer agreement.

SUPPLEMENTARY MATERIALS

www.sciencemag.org/content/360/6395/eaao4927/suppl/DC1
Figs. S1 to S15
Table S1

27 July 2017; accepted 27 April 2018
10.1126/science.aao4927

Science

In vivo brain GPCR signaling elucidated by phosphoproteomics

Jeffrey J. Liu, Kirti Sharma, Luca Zangrandi, Chongguang Chen, Sean J. Humphrey, Yi-Ting Chiu, Mariana Spetea, Lee-Yuan Liu-Chen, Christoph Schwarzer and Matthias Mann

Science **360** (6395), eaao4927.
DOI: 10.1126/science.aao4927

Mechanisms of drug action

Advanced mass spectrometry methods enable monitoring of tens of thousands of phosphorylation sites in proteins. This technology can potentially distinguish cellular signaling pathways that produce beneficial effects from those that produce unwanted side effects. Liu *et al.* treated mice with various agonists of the kappa opioid receptor (a G protein–coupled receptor) and monitored changes in phosphorylation over time in different brain regions. The phosphorylation patterns revealed distinct patterns of signaling in various brain tissues, some of which were associated with unwanted side effects.

Science, this issue p. eaao4927